Supporting information for -

Programming layer-by-layer liquid phase epitaxy in microfluidics for realizing two-dimensional metal-organic framework sensor arrays

Huijie Jiang[a], Bo Cheng[a], Joachim Knoch[b], Sandeep Kumar[c,d], Neeraj Dilbaghi[d], Akash Deep[e,f], Sven Ingebrandt[a], Vivek Pachauri[*a]

[a]Institute of Materials in Electrical Engineering 1, RWTH Aachen University, Sommerfeldstrasse 24, 52074 Aachen, Germany.

[b]Institute of Semiconductor Electronics, RWTH Aachen University, 52074 Aachen, Germany

[c]Department of Physics, Punjab Engineering College (Deemed to be University), Chandigarh, 160012 India

[d]Department of Biotechnology, Guru Jambheshwar University of Science and Technology, Hisar 125001, India

[e]Academy of Scientific and Innovative Research (AcSIR), Ghaziabad 201002, Uttar Pradesh, India

[f]Institute of Nano Science and Technology (INST), Sector-64, Mohali 160062, Punjab, India

Corresponding author: Dr. Vivek Pachauri: pachauri@iwe1.rwth-aachen.de

Figure S1. Photograph showing the automated and programmable microfluidic platform realized for the growth of 2D Ni-MOF using LbL-LPE. The platform includes the use of programmable pumps from Labsmith™ with high accuracy control of fluidic volumes.

Figure S2. Optical contrastometry based thickness evaluation of the 2D Ni-MOF grown on Si/SiO_2 substrates. (a) The trilayer stacking of the SiO_2/Ni-MOF/Air interface with a finite thickness of SiO_2 on Si achieved by thermal oxidation serving as an optical reference. (b) The graph shows an optical contrast calibration prepared for different thicknesses of 2D Ni-MOF obtained via dip coating method. This optical contrast calibration allows for a simple and accurate approach to carry out thickness and homogeneity determination of the growth MOF layers on the given reference substrate (Si/SiO_2 in this case).

Figure S3. Sensor chip configuration used for the realization of 2D Ni-MOF devices using LbL-LPE for the electrical impedance spectroscopy based detection of diisobutyl phthalate. (a) A complete layout of the sensor chip which shows four units comprised of six source-drain microelectrode arrays each. In total, therefore, there are 24 devices on the chip. Each chip measures 15 mm by 10 mm. In this configuration, a common source electrode is connected to all the sensor devices, which drains electrodes are individually addressed to carry out the measurement for each device (b) A typical device configuration employed for the sensor chip is shown where purple colour shows the source and drain interdigitated microelectrodes, while the red region is the active channel realized by the 2D Ni-MOF growth. Each device region overall measures 200 µm by 300 µm. With a total of 16 microelectrodes, each device exhibits an effective channel width of 6400 µm and 13 µm in length (c) A zoomed in region from the sensor device shows the width of the interdigitated microelectrodes and the gap in between. The mask layout for the lithography was prepared in CleWin™ 3.0.

Figure S4. Photographic image of a typical microfluidic chip used for the programmable LbL-LPE growth of 2D Ni-MOF. The chip is housed in the white mould prepared using 3D printing, PDMS layer with housed the microfluidic channel, which is homogeneously pressed against the chip using the specially designed clamp that ensured equal pressure throughout the PDMS layer.

Figure S5. Surface characterizations of LbL-LPE grown 2D Ni-MOFs using scanning electron microscopy. Images (a) to (d) show the 2D Ni-MOF synthesized after 10, 15, 20 and 25 growth cycles in the microfluidic circuit. All the images show a homogeneous growth of 2D Ni-MOF and smooth topographic characteristics. Scale bar is 400 nm.

Figure S6. Atomic force microscopy (AFM) images of Ni-MOFs with 10c, 15c, 20c and 25c LbL cycles.

Figure S7. GIXRD pattern of 80c Ni-MOF grown using a LbL-LPE approach. Two peaks located at 10.2^o and 17.5^o are ascribed to Ni-MOF. The broad peak centralized at 25^o and sharp peak at 33^o are contributed by SiO_2 and Si substrate, respectively.

Figure S8. Transmission electron microscopy (TEM) images. (a) A TEM image of Ni-MOF particle clusters scratched from Si/SiO_2 substrate. (b) A high-resolution TEM image with lattice fringes. Insert is the corresponding FFT (FFT = Fast Fourier Transform) image.

Figure S9. High resolution SEM characterization of the 2D Ni-MOF growth on Au microelectrodes. Left side image: The SEM scan images Ni-MOF grown over Si/SiO_2 and Au substrate where the change in contrast represents the border. Right side image shows the topography of the 2D Ni-MOF grown on Au electrode.

Figure S10. Sensor response reproducibility of 2D Ni-MOF based devices for the detection of phthalate molecules in water. Nyquist plots of 6 different individual devices on a sensor chip are shown here in the graphs.

Table S1. Optimization of 2D Ni-MOF growth parameters at 20 LbL cycles.

Table S2. Fitted values for four different concentrations of DiBP on the same 2D Ni-MOF sensor chip with 20 LbL cycles.

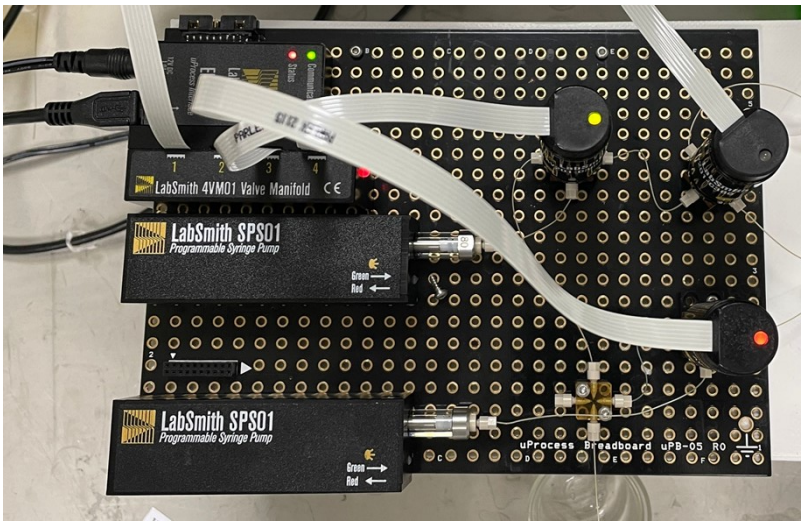

Figure S1. Photograph showing the automated and programmable microfluidic platform realized for the growth of 2D Ni-MOF using LbL-LPE. The platform includes the use of programmable pumps from Labsmith™ with high accuracy control of fluidic volumes.

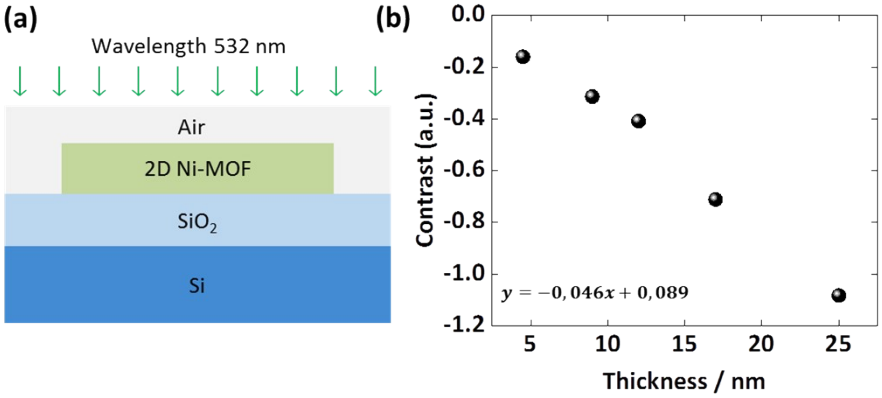

Figure S2. Optical contrastometry based thickness evaluation of the 2D Ni-MOF grown on Si/SiO_2 substrates. (a) The trilayer stacking of the SiO_2/Ni-MOF/Air interface with a finite thickness of SiO_2 on Si achieved by thermal oxidation serving as an optical reference. (b) The graph shows an optical contrast calibration prepared for different thicknesses of 2D Ni-MOF obtained via dip coating method. This optical contrast calibration allows for a simple and accurate approach to carry out thickness and homogeneity determination of the growth MOF layers on the given reference substrate (Si/SiO_2 in this case).

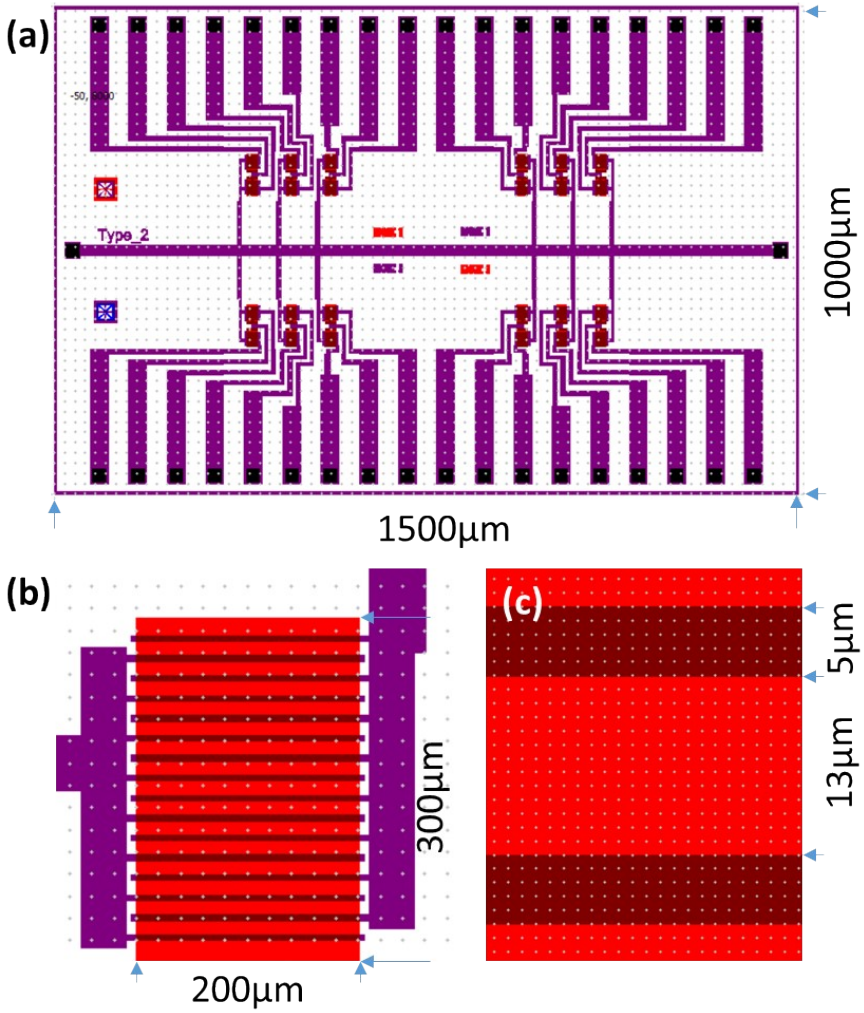

Figure S3. Sensor chip configuration used for the realization of 2D Ni-MOF devices using LbL-LPE for the electrical impedance spectroscopy based detection of diisobutyl phthalate. (a) A complete layout of the sensor chip which shows four units comprised of six source-drain microelectrode arrays each. In total, therefore, there are 24 devices on the chip. Each chip measures 15 mm by 10 mm. In this configuration, a common source electrode is connected to all the sensor devices, which drains electrodes are individually addressed to carry out the measurement for each device (b) A typical device configuration employed for the sensor chip is shown where purple colour shows the source and drain interdigitated microelectrodes, while the red region is the active channel realized by the 2D Ni-MOF growth. Each device region overall measures 200 µm by 300 µm. With a total of 16 microelectrodes, each device exhibits an effective channel width of 6400 µm and 13 µm in length (c) A zoomed in region from the sensor device shows the width of the interdigitated microelectrodes and the gap in between. The mask layout for the lithography was prepared in CleWin™ 3.0.

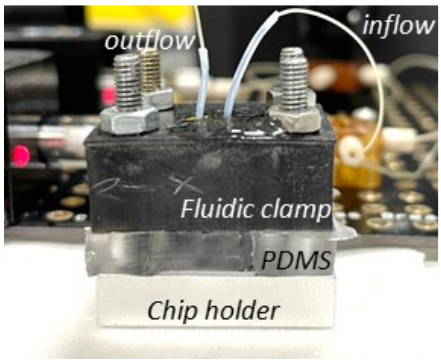

Figure S4. Photographic image of a typical microfluidic chip used for the programmable LbL-LPE growth of 2D Ni-MOF. The chip is housed in the white mould prepared using 3D printing, PDMS layer with housed the microfluidic channel, which is homogeneously pressed against the chip using the specially designed clamp that ensured equal pressure throughout the PDMS layer.

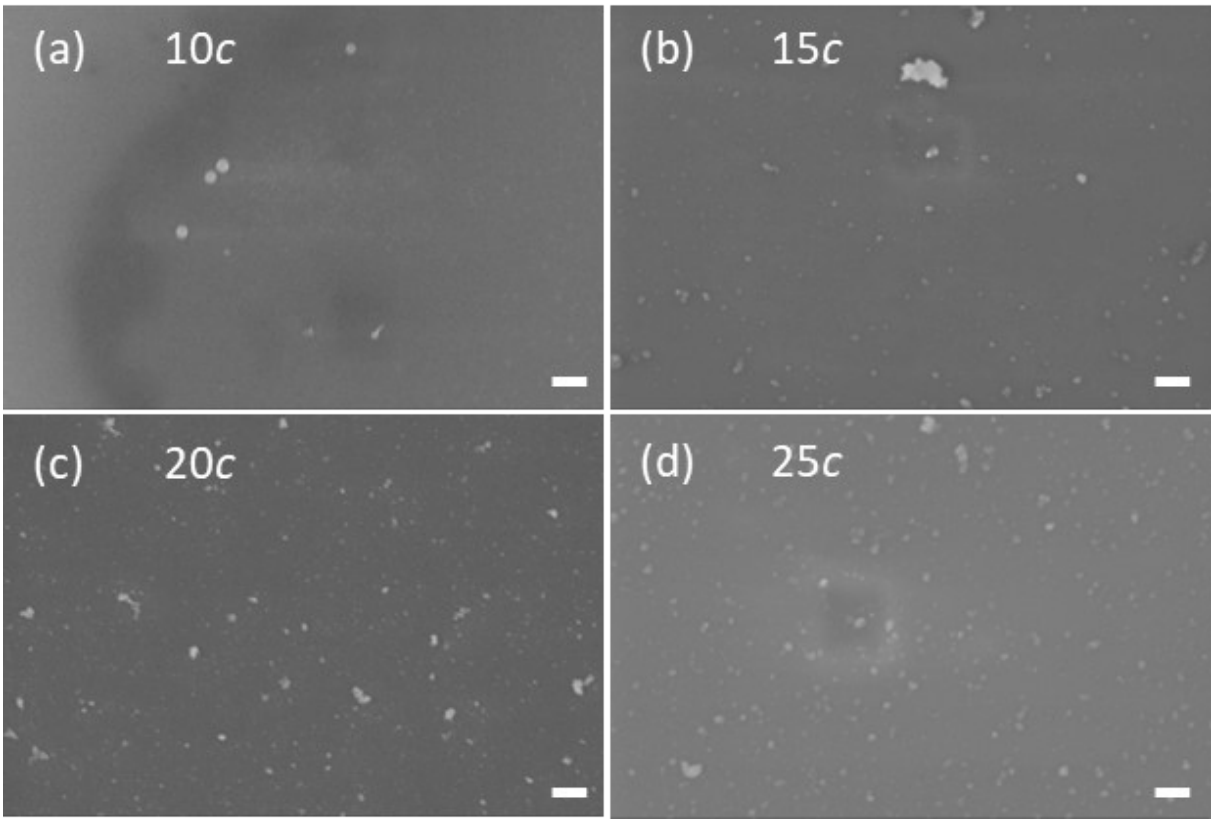

Figure S5. Surface characterizations of LbL-LPE grown 2D Ni-MOFs using scanning electron microscopy. Images (a) to (d) show the 2D Ni-MOF synthesized after 10, 15, 20 and 25 growth cycles in the microfluidic circuit. All the images show a homogeneous growth of 2D Ni-MOF and smooth topographic characteristics. Scale bar is 400 nm.

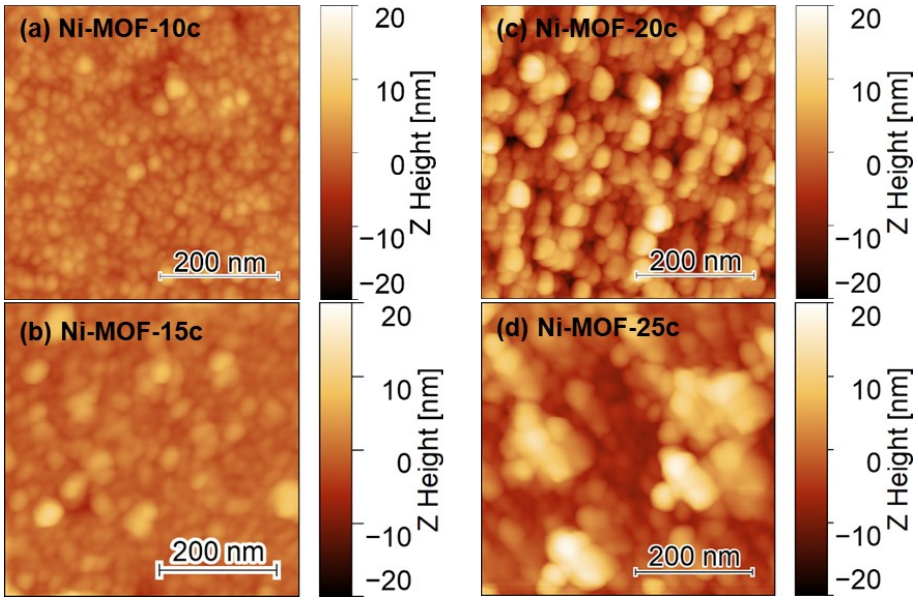

Figure S6. Atomic force microscopy (AFM) images of Ni-MOFs with 10c, 15c, 20c and 25c LbL cycles.

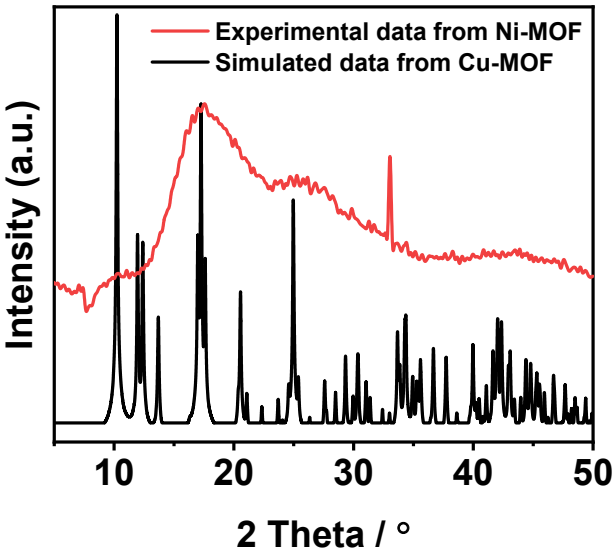

Figure S7. GIXRD pattern of 80c Ni-MOF grown using the LbL-LPE approach and the theoretical XRD pattern of Cu-MOF (or Cu-BDC). Ni-MOF is expected to have a similar crystallographic structure as Cu-MOF. The two peaks located at 10.2° and 17.5° are ascribed to Ni-MOF and their relatively broad shape are likely a consequence of the nanoscale grain sizes of Ni-MOF as shown in AFM analysis. The broad peak centralized at 25° and sharp peak at 33° are contributed by SiO_2 and Si substrate, respectively.

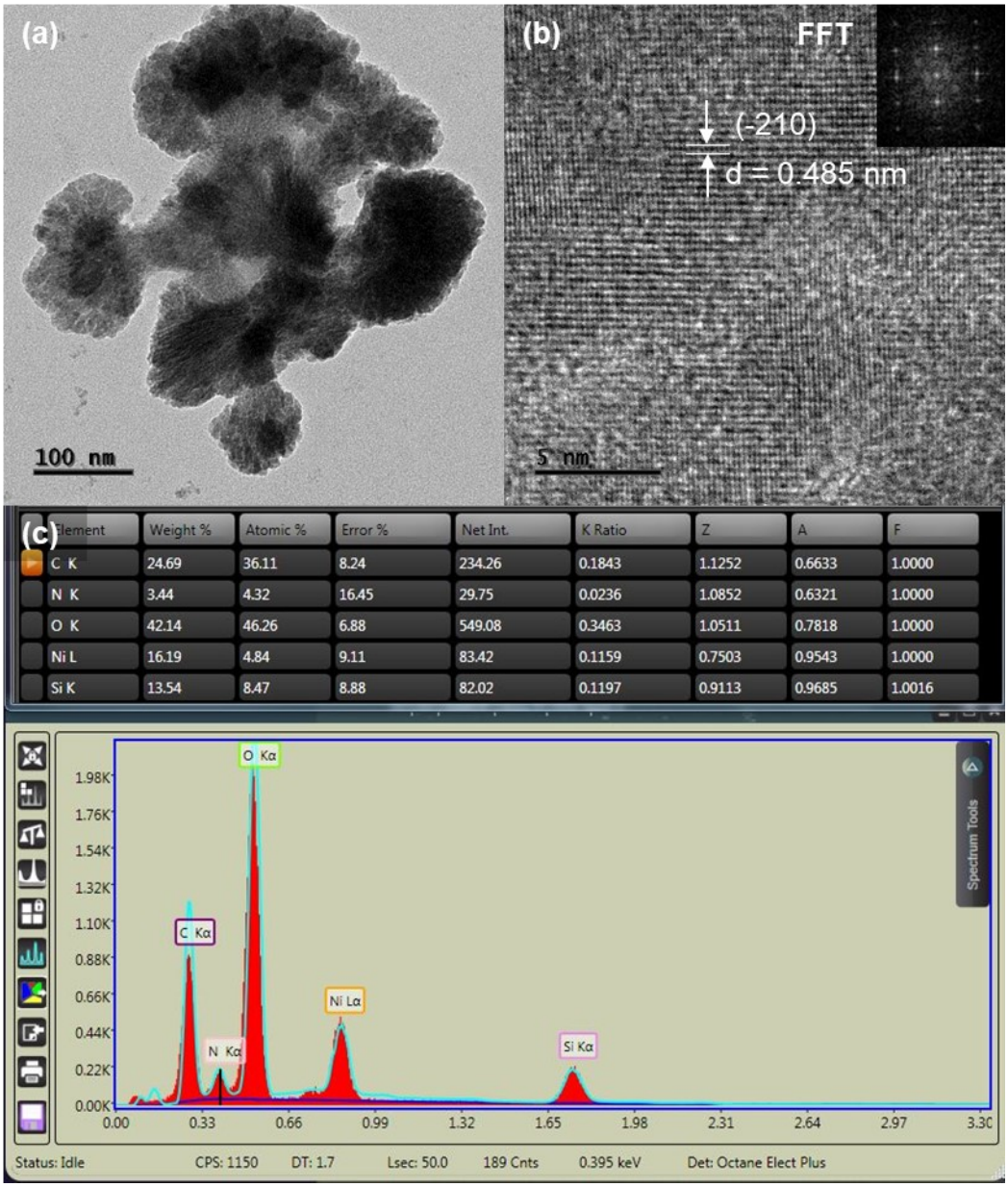

Figure S8. (a) A TEM image of Ni-MOF thin film material as scratched from Si/SiO_2 substrate. (b) A comprehensive analysis of the high-resolution TEM image shows the distance between two adjacent fringes to be 0.485 nm when applying FFT and inverse FFT, which is attributed to the Miller plane of (-210). The corresponding diffraction angle can be calculated to 2θ = 18.2°, which is in accordance with the XRD result (fig. S7). (c) Table above shows the composition of the Ni-MOF characterized by using SEM-EDX spectra and corresponding weight and atomic percentage of Ni, C and N elements. Herein, the contents of Si and O elements may not be accurate due to the influence from Si/SiO_2 substrate. The relative atomic ratios of Ni to N elements and C to N elements were determined to be 1.12 and 8.36, respectively, which are in good agreement with the reported Ni-MOF.[1]

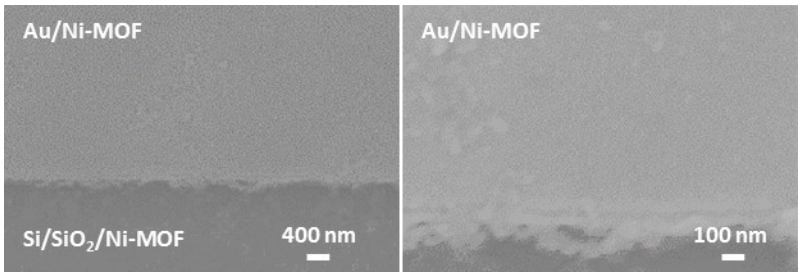

Figure S9. High resolution SEM characterization of the 2D Ni-MOF growth on Au microelectrodes. Left side image: The SEM scan images Ni-MOF grown over Si/SiO_2 and Au substrate where the change in contrast represents the border. Right side image shows the topography of the 2D Ni-MOF grown on Au electrode.

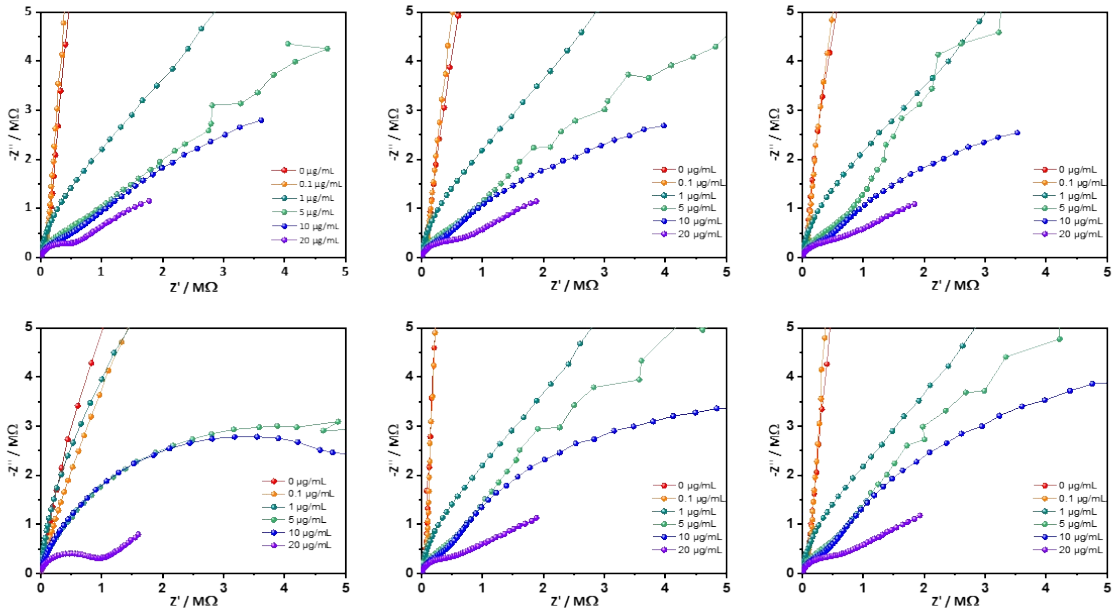

Figure S10. Sensor response reproducibility of 2D Ni-MOF based devices for the detection of phthalate molecules in water. Nyquist plots of 6 different individual devices on a sensor chip are shown here in the graphs.

Table S1. Optimization of 2D Ni-MOF growth parameters at 20 LbL cycles.

Parameters	**Value 1** **Ra / nm**	**Value 2** **Ra / nm**	**Value 3** **Ra / nm**
Metal concentration [mM]	0.5 0.38	0.75 0.282	1 0.274
Organic concentration [mM]	0.5 0.312	0.75 0.296	1 0.284
Metal volume [µL]	40 0.296	80 0.269	120 0.272
Organic volume [µL]	40 0.266	80 0.3	120 0.227
Clean volume [µL]	80 0.296	160 0.272	240 0.269
Precursor flow [$\mu L \cdot min^{-1}$]	2.5 0.256	6 0.237	8 0.271
Clean flow [$\mu L \cdot min^{-1}$]	80 0.321	200 0.312	400 0.344

Table S2. Fitted values for four different concentrations of DiBP on the same 2D Ni-MOF sensor chip with *20 LbL cycles*.

Concentration / (µg/mL)	**R_s / Ω**	**R_{ct} / Ω**	**C_{dl} / nF**	**Q / µT**	**n**
1	9042	2.97E5	0.013	0.0004	0.682
5	9069	4.44E5	0.013	0.006	0.498
10	7062	2.89E5	0.014	0.010	0.488
20	8014	3.78E5	0.015	0.028	0.464

S11. Calculation of the limit of detection and comparison of sensor performance

The LoD is calculated based on the following formula:

$(Q_A)_{LOD} = Q_{mb} + 3\sigma_{mb}$

Where $(Q_A)_{LOD}$ is the minimal signal that would be detected, Q_{mb} and σ_{mb} are the mean value and standard deviation of reference measurements?

Here, in this case, $(Q_A)_{LOD}$ = (1.69 x 10^{-4} + 3 x 8.65 x 10^{-5}) µT = 4.285 x 10^{-4} µT.

Then, the LOD of detection is determined by plugging $(Q_A)_{LOD}$ in the calibration curve of

Log(Q) = 0.104 x Conc – 3.42

to be 0.5 µg/mL.

The following chart presents the reported LODs based on electrochemical impedance spectroscopy. The LOD reported in this work is higher, which is probably due to the low conductivity of Ni-MOF compared with graphene and conductive polymers, as well as the difference in device layout. For instance, in this work we employ Ni-MOF sensor arrays in micro scale for the detection of DiBP, while the other reported researches using glassy carbon electrode (GCE), which is in millimetre scale.

Phthalates	**Materials**	**Limit of detection**	**Ref.**
DBP	MIP PPY/PGE	1.3 ng/mL	2
DEP	Graphene/GCE	0.024 pg/mL	3
DEHP	graphene–β-cyclodextrin/GCE	48.9 ng/mL	4
DBP	antigen/ chitosan/MWCNTs@GONRs/GCE	7 ng/mL	5
DiBP	Ni-MOF sensor arrays	500 ng/mL	This work

References:

1. Y.-J. Shih, Z.-L. Wu and J.-Z. Luo, Appl. Catal B- Environ Energy, 2024, 357.
2. G. Bolat, Y. T. Yaman, S. Abaci, Sens. Actuators. B Chem, 2019, 299, 127000.
3. X. Jiang, Y. Xie, D. Wan, F. Zheng, and J. Wang, *Sensors.* 2020, *20* (3), 901.
4. S. Xiong, J. Cheng, L. He, M. Wang, X. Zhang, Z. Wu, Anal. Methods, 2014, 6, 1736.
5. Y.-R. Liang, Z.-M. Zhang, Z.-J. Liu, K. Wang, X.-Y. Wu, K. Zeng, H. Meng, Z. Zhang, Biosens. Bioelectron., 2017, 91, 199.